Characterization of an Optical Pulse Slicer for Gas-Phase Electric Field Measurements Using Field-Induced Second Harmonic Generation

Tat Loon Chng, C. Ding, M. Naphade, B.M. M Goldberg, I.V. V Adamovich, Svetlana Starikovskaia

Characterization of an Optical Pulse Slicer for Gas-Phase Electric Field Measurements Using Field-Induced Second Harmonic Generation

T. L. Chng,[a,*] Ch. Ding,[a] M. Naphade,[b] B. M. Goldberg,[c] I. V. Adamovich[d] and S. M. Starikovskaia[a]

[a] *Laboratory of Plasma Physics (CNRS, Ecole Polytechnique, Sorbonne Universities, University of Pierre and Marie Curie - Paris 6, University Paris-Sud), Ecole Polytechnique, route de Saclay, 91128 Palaiseau, France*

[b] *Department of Mechanical and Aerospace Engineering, Princeton University, Princeton, NJ 08544, USA*

[c] *Combustion Research Facility, Sandia National Laboratories, Livermore, California, 94551, USA*

[d] *Nonequilibrium Thermodynamics Laboratories, Department of Mechanical and Aerospace Engineering, Ohio State University, Columbus, OH 43210, USA Name of Institute, Address, Country*

E-mail: tat-loon.chng@lpp.polytechnique.fr

ABSTRACT: This work describes the characterization of an optical pulse-slicer for performing electric field measurements using the Electric Field Induced Second Harmonic generation (or E-FISH) method. This laser-based diagnostic generally favors ultrashort (sub-nanosecond) pulses, given their intrinsically higher intensities and superior measurement time resolution. However, such laser systems can often prove inaccessible due to their high costs. Our response to this problem is to develop a Pockels-cell-based pulse slicing scheme, compatible with the more affordable and ubiquitous class of nanosecond laser sources. Using such a slicer, we demonstrate the ability to slice a 35 mJ, 20 ns (FWHM), 1064 nm pulse from a conventional Nd:YAG laser down to about 3 ns (FWHM) with an energy of 2 mJ. These shorter pulses are in turn used to make electric field measurements in an electrostatic field (at 5 bar) using E-FISH. Measurements performed with these sliced pulses not only have the expected benefit of improving the time resolution of the field measurement, but also reduce the possibility of laser-plasma interactions due to the lower laser pulse energy required. The current pulse slicer incorporates an off-optimum design Pockels cell, which limits the minimum pulse width and maximum energy that may be realized. It is anticipated that higher energies and a reduction in the pulse width to around 100 ps may be achieved with further optimization, and could present a cost-effective approach to extending the applicability of the E-FISH method.

KEYWORDS: Electric field measurements; Optical second harmonic generation; Pockels cell.

* Corresponding author.

Contents

1. Introduction

Electric field induced second harmonic generation, or E-FISH, is a non-linear optical method developed around the 1970's, which has been applied to a wide variety of problems. These include the measurement of gas hyperpolarizabilities [1], detection of terahertz radiation [2], and even as a weakly coupled, non-intrusive optical probe for examining the focal region of a laser beam [3]. More recently, this method has seen somewhat of a resurgence in interest, primarily for its promise as an effective electric field measurement tool for gas discharges and plasmas [4-5]. The essence of an E-FISH experiment involves probing a centrosymmetric gas sample with laser light at a fundamental frequency ω, and quantifying its second harmonic response (i.e. at frequency 2ω) to an externally applied electric field which is to be measured. The intensity of this second harmonic signal varies quadratically with the applied field strength, and is otherwise absent if no field is imposed. It is worth emphasizing that the E-FISH signal is generated coherently, and co-propagates together with the fundamental probe beam. This path-integrated, coherent signal is then easily isolated (from the fundamental) using a dispersive prism or a dichroic mirror. Calibration may be performed in a known electrostatic field, so as to obtain absolute field information in a plasma. Electric field measurements using E-FISH have since been successfully performed in various discharge geometries, such as a fast ionization wave cylindrical tube discharge [6], a pin to plane discharge [7], and a nanosecond dielectric barrier discharge (DBD) [8]. The possibility of obtaining 1-D field information by focusing the laser light with a cylindrical lens has also been recently demonstrated [9].

An important advantage of the E-FISH method which is of relevance to the present work, is the fact that the signal generation is effectively instantaneous, and therefore only physically limited by the duration of the probe beam. Excellent temporal resolution is thus readily achieved using picosecond or femtosecond pulses. This feature is particularly attractive in non-equilibrium plasmas, a term frequently used to describe plasmas in which the electron temperature is elevated to several orders of magnitude more than the gas temperature [10]. These plasmas are typically initiated by high-voltage pulses with a characteristic rise time of a few nanoseconds, and pulse widths between a few to hundreds of nanoseconds. Non-equilibrium plasmas have been the

subject of significant research interest over the last decade or so, given their ability to alter the chemical reactivity of a system, and have been incorporated into applications covering a wide range of disciplines such as biology, medicine, combustion and agriculture [11-13]. Studies have found that the generation of extremely large and rapidly evolving electric field transients is the main mechanism responsible for realizing this enhanced chemical reactivity [14-15]. There is therefore substantial interest in developing non-intrusive measurement techniques capable of quantifying and resolving the temporal character of these fields.

The above discussion supports the use of shorter, sub-nanosecond laser pulses as a way of exploiting the excellent time resolution afforded by the E-FISH diagnostic. Furthermore, for the same energy, shorter pulses imply a higher intensity, and lead to stronger signals as shown below in eqn. (2). However, a common drawback associated with these ultrashort pulse systems is their inaccessibility, primarily due to their exorbitant costs. This has motivated the development of an optical pulse slicing scheme, which provides the capability of reducing the temporal width of a long laser pulse to one of a suitably shorter duration. The idea is that such a pulse slicer should be readily compatible and easily integrated into more accessible and affordable laser systems (for e.g. nanosecond lasers), so that the benefits of operating in a shorter pulse regime may be extended to a wider audience. The present work describes the characterization of a Pockels-cell-based pulse slicer, for the specific purpose of performing E-FISH measurements in a plasma. The following section describes this characterization in greater detail, while section 3 discusses some of the E-FISH results obtained using this slicer.

2. Experimental setup

The experimental setup consists of 3 parts, the optical layout (including the Pockels cell) for the pulse-slicing, the corresponding optical layout for the E-FISH measurements, and the high voltage (HV) pulser and discharge cell used for conducting the E-FISH measurements.

2.1 Pulse slicer characterization and optical layout

Figure 1 shows a schematic of the pulse slicing scheme developed in this work. This slicer is integrated with a conventional Quanta-Ray Lab-230, Q-switched, nanosecond Nd:YAG laser system, which acts as a source of 1064 nm, 16 ns (FWHM) pulses, with an energy of about 200 mJ per pulse at a repetition rate of 10 Hz. These pulses, which are slightly elliptically polarized, are first directed through a polarizing cube, PBS1, to achieve the linear polarization required for the E-FISH experiments. A half-wave plate, polarizing cube pair (denoted as HWP and PBS2 respectively) is then used to attenuate the 240 mJ beam to about 50 mJ before entering the Pockels cell. Reducing the pulse energy in this way provides better shot–to–shot energy and pulse width stability.

The Pockels cell is the crucial active element within the pulse slicer. It essentially functions as an electronic wave plate; applying a sufficiently high voltage across the cell alters the birefringence of the cell material, and thereby rotates the polarization of the light passing through. The linear relationship between the applied voltage and the induced birefringence is the well-known Pockels effect. It should be added that this polarization response occurs instantaneously and lasts for as long as the high voltage is sustained across the cell. One may in turn take advantage of this idea as a method for pulse slicing, by simply placing a Pockels cell in between two crossed polarizers, such as PBS2 and PBS3 shown in figure 1. In the absence of any high voltage (this is termed the “OFF” state), any CW light which passes through the first polarizer (PBS2) is blocked by the second (PBS3). However, applying a high voltage across the Pockels cell (i.e. the “ON”

state), allows some light to be transmitted through PBS3. More importantly, if this high voltage is delivered in the form of a short pulse, then it follows that the resulting transmitted output will acquire a temporal profile which closely matches that of the applied high-voltage waveform [16]. For optimum performance, the Pockels cell should be aligned for maximum transmission before the second polarizer (i.e. PBS3) when in the "OFF" state. Typically the electric field vector across the cell should be parallel to the polarization of the light passing through the first polarizer (i.e. PBS2).

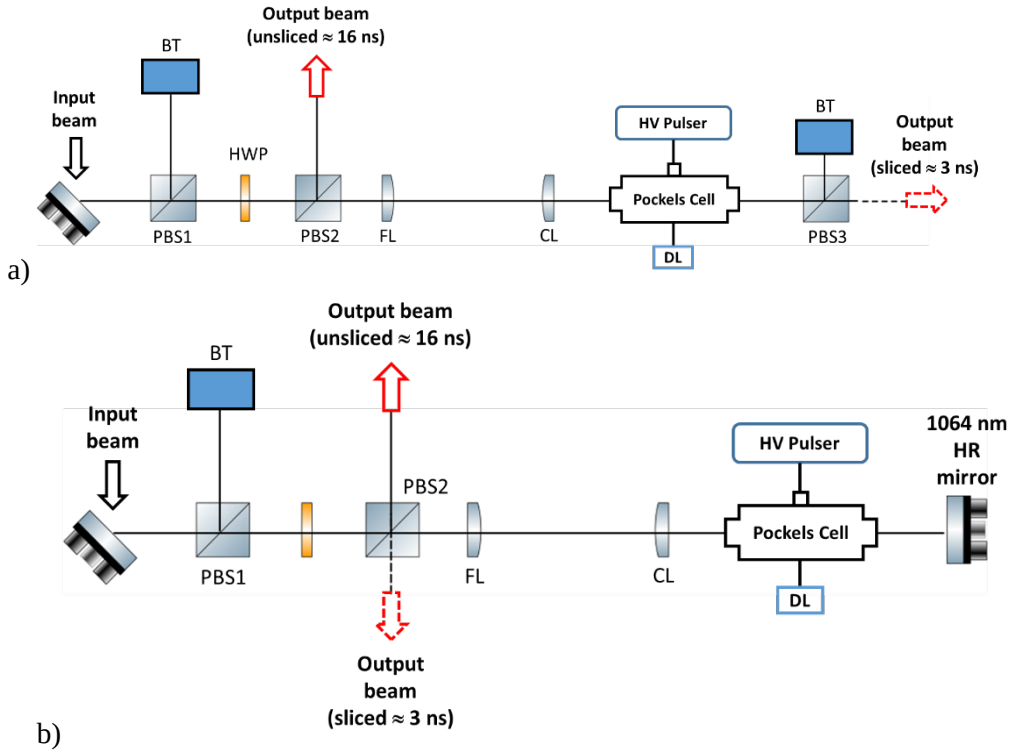

Figure 1. Schematic of the a) single-pass and b) double-pass pulse-slicing scheme.

The Pockels cell used in these experiments is supplied by Leysop Ltd and consists of a UV BBO crystal mounted within a custom-made housing with electrical leads. The cell is driven by a FID high voltage generator (model number FDS 3-1NM1) capable of delivering up to 3 kV pulses with a nominal pulse width of 2 ns (FWHM). These pulses are delivered to the cell and terminated with a matching 50 Ω dummy, high voltage load (DL). The cell may therefore be treated as a small shunt capacitance within a 50 Ω resistance line. It is important to point out that the housing is carefully designed so as to (i) provide an electrical interface which minimizes distortions to the high voltage pulses and (ii) avoids initiating electrical breakdown of the surrounding air. The cell has an entrance diameter of about 4 mm, substantially smaller than the 10 mm diameter of the 1064 nm beam. A positive-negative lens pair (denoted as FL and CL respectively) is used to reduce the beam diameter so as to match the entrance aperture of the cell.

As discussed earlier, the width of the applied high voltage pulses limits the minimum optical pulse width which may be achieved. To characterize this response, a CW red diode laser is passed through the slicer and the resulting output captured with a Thorlabs DET10A, 1 ns rise time photodiode. Figure 2a shows that the idealized CW response of the cell at maximum driving voltage is about 2 ns. Performing this test also serves the purpose of detecting any spurious electrical reflections which may exist within the circuit.

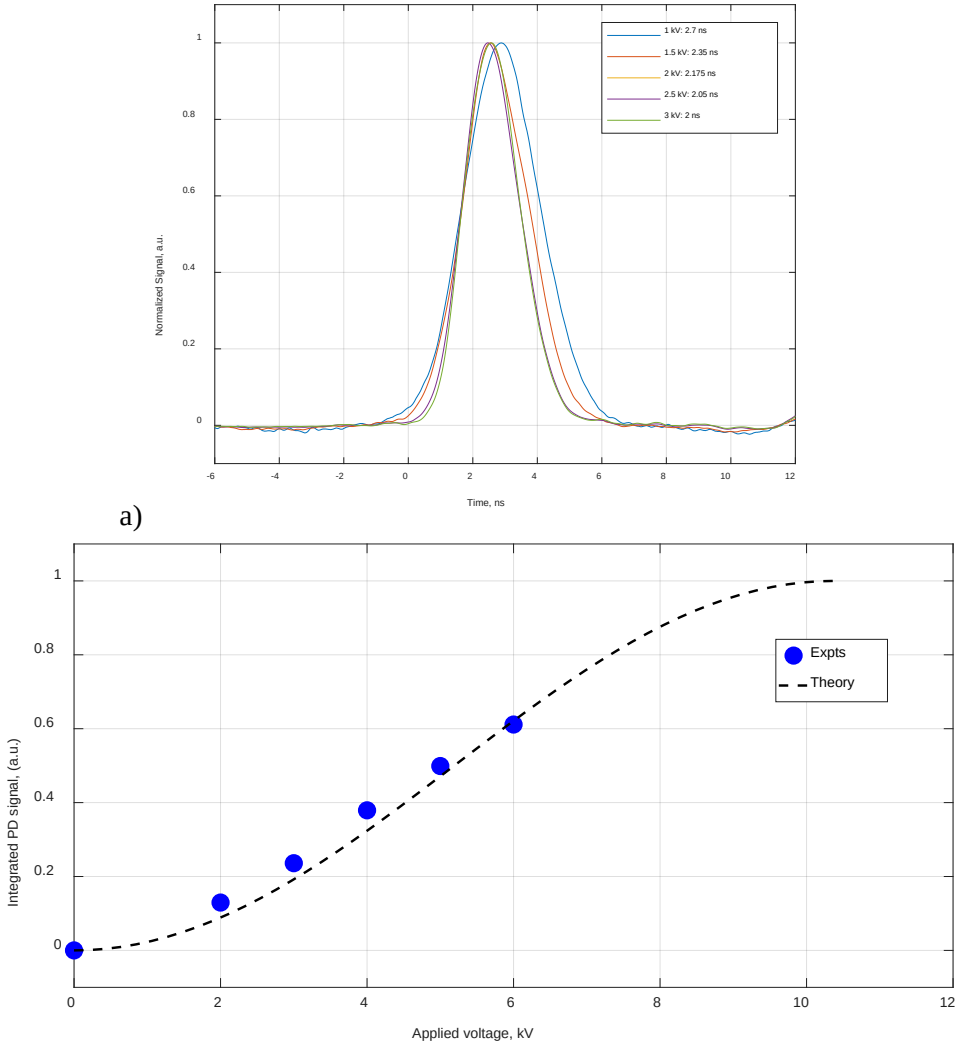

Figure 2. Pockels cell response as a function of driving voltage with a) CW red diode laser (temporal waveforms) and b) 1064 nm, 16 ns (FWHM) laser pulse (integrated photodiode signals). Integrated signals are rescaled by a constant factor in order to fit the theoretical values predicted by eqn. (1)

It may be inferred from figure 1a that maximum throughput is obtained when the Pockels cell is able to effect half-wave rotation, i.e. rotate the polarization of the input light by 90°. This is mathematically described by eqn. (1), which indicates that optimal output, A is attained when the applied voltage, V is equal to the half-wave voltage, V_{HW}. (B is just a cell-dependent proportionality constant.)

$$A = B \cdot sin^2\left(\frac{\pi}{2} \cdot \frac{V}{V_{HW}}\right) \quad (1)$$

For most crystals, this half-wave voltage is approximately linearly proportional to the wavelength of the incident light. Unfortunately, the UV BBO crystal used in our Pockels cell was specifically designed for operation at 205 nm, which implies a half-wave voltage that is at least a factor of 5 smaller than at 1064 nm. This limits the amount of energy that can be obtained due to an inability to achieve half-wave rotation at 1064 nm, and also restricts the energy input to the cell given the risk of damage to the wavelength-specific optical coatings.

In order to mitigate this problem, a double-pass configuration is implemented by replacing PBS3 with a highly reflecting 1064 nm mirror as shown in figure 1b. Such a configuration effectively doubles the voltage delivered to the Pockels cell and hence results in a larger polarization rotation. For this arrangement to work, it is important to ensure that the round trip time through the cell is less than the width of the applied high voltage pulse. Figure 2b shows the output obtained from the cell as a function of driving voltage for the double-pass configuration. Since the driving voltage is still below the half-wave voltage, increasing the applied voltage continues to raise the energy of the output from the cell. Good agreement is obtained between experiments and the values predicted by eqn. (1). The half-wave voltage for 1064 nm used in eqn. (1) is assumed to be 10 kV, which is about 5 times larger than the half-wave voltage at 205 nm (i.e. 2 kV). As a consequence of the double-pass configuration, the effective applied voltage is twice that of the actual applied voltage.

Using the Pockels cell to slice a longer pulse (as opposed to a CW beam) additionally requires that the cell is triggered in coincidence with the temporal peak of the incident pulse. For optimum performance, the constraints on the timing accuracy become more stringent as the desired pulse width is reduced. Figure 3 shows that sub-nanosecond timing accuracy is required to optimize the energy output. In arriving at these results, the high voltage generator which drives the Pockels cell is slaved to the Q-switch of the Nd:YAG laser, and the time delay is varied in steps of about 250 ps.

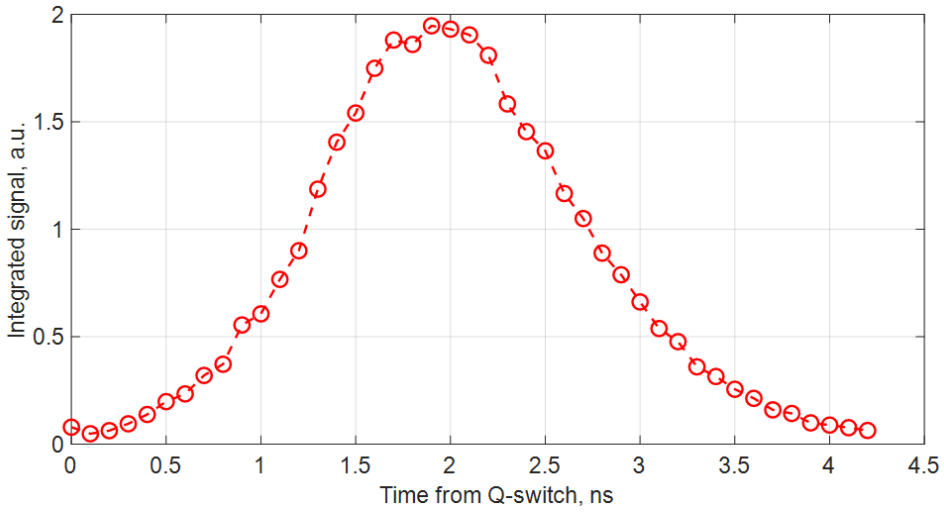

Figure 3. Energy output from pulse slicer (averaged over 200 laser shots) as a function of the timing delay between the triggering of the Pockels cell and the Nd:YAG laser Q-switch.

Compared with the single-pass configuration, the double-pass scheme achieves a higher output energy, without any detriment to the pulse width. Both these waveforms are shown in figure 4. However, a comparison of the input and output profiles shows that the pulse slicing process appears to alter the shape of the laser pulse. This is probably due in part to the inability of the Pockels cell to achieve full half-wave rotation. Additionally, the width of these sliced laser pulses (~2.8 ns) are also observed to be slightly longer than that measured with the CW beam (~2 ns). This is likely to be related to the temporal variation in energy associated with using an input laser pulse as opposed to a CW beam.

Given its superior performance, the double-pass configuration is used for the E-FISH experiments. This pulse slicer converts a 50 mJ, 16 ns (FWHM) laser pulse into a shorter 2.8 ns (FWHM) pulse with an energy of about 2 mJ. This represents an energy efficiency of about 4%,

a figure which could be easily improved with a Pockels cell dedicated for 1064 nm wavelength operation. The extinction ratio of the slicer, defined as the ratio of the output energy in the "ON" versus the "OFF" state, is measured to be about 1% and is found to have no influence on the E-FISH experiments.

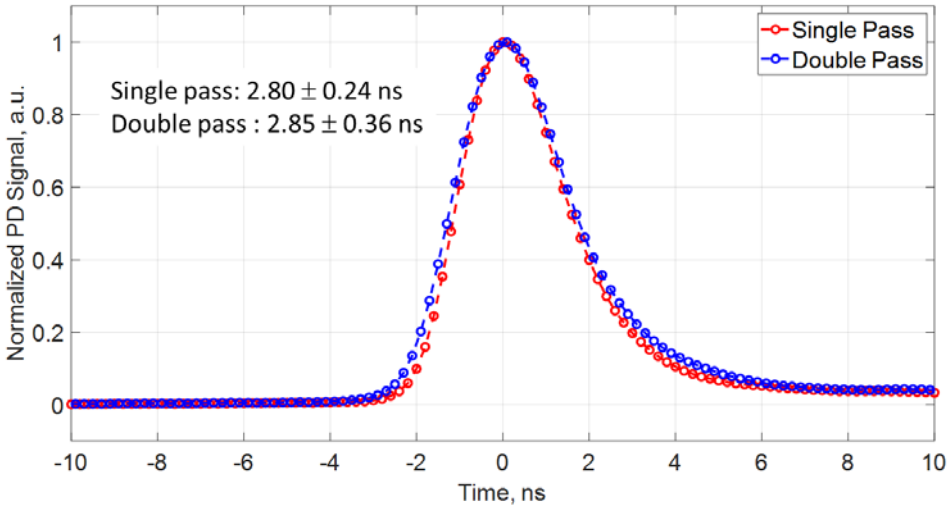

Figure 4. Sliced pulse waveforms obtained with the single versus double-pass configuration.

2.2 E-FISH optical layout

The setup for the E-FISH experiments is very similar to that used in our previous studies and will therefore only be briefly described here. As shown in the figure 5, the vertically polarized, 2.8 ns sliced pulse is focused with a f = 150 mm (FL1) lens into the discharge cell. (The resulting confocal beam parameter, estimated based on a Gaussian beam approximation, is about 2.4 mm.) The co-propagating 1064 nm light and the 532 nm second harmonic signal are collimated with a f = 250 mm lens (FL2), and separated with a dichroic mirror (DM) and an equilateral dispersive prism (DP). The vertically polarized component of this second harmonic signal is isolated with a 532 nm polarizing cube (PBS), and focused with a f = 150 mm lens (FL3) onto a Hamamatsu (model number H7422-50P) PMT. A 532 nm centered, 10 nm FWHM bandpass filter (BP) is attached to the entrance of the PMT for stray light rejection. Finally, part of the residual 1064 nm light which reflects off the dichroic mirror is directed onto a 1 ns rise time photodiode (PD) and used as a monitor of the laser intensity (see eqn. (2)).

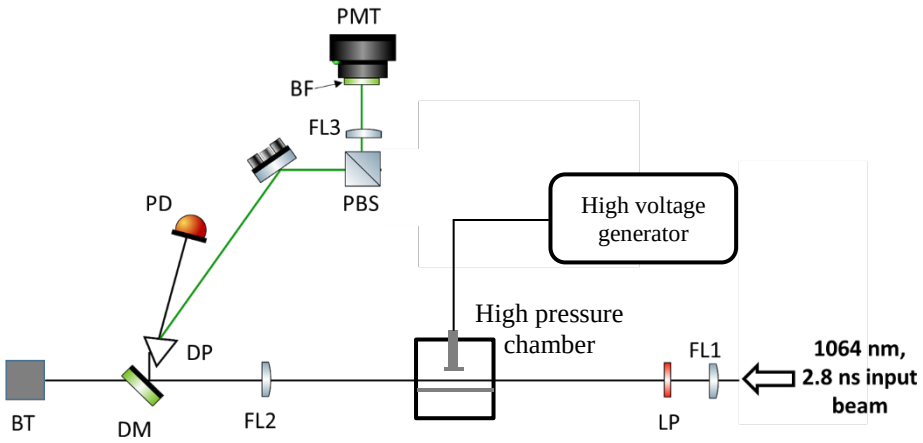

Figure 5. Schematic of the E-FISH optical setup.

2.3 High pressure cell

The high pressure cell used in these experiments is a slightly modified version of a high-pressure chamber constructed specially for plasma assisted combustion related studies [17]. The chamber can withstand working pressures of up to 12 bar and as shown in figure 6, has 3 circular viewing ports to facilitate spectroscopic measurements. The electrode geometry is modified such that the high voltage electrode consists of an aluminum disk (20 mm in diameter) while the grounded electrode is a larger 46 mm diameter aluminum plate. The interelectrode gap distance is maintained at 5 mm.

The high-voltage electrode is connected to the central wire of a 30 m long, 50 Ω coaxial cable by a metal rod situated on the axis of symmetry of the cylindrical system, while the other end of the cable is connected to a high voltage generator. Negative polarity, 12 kV amplitude, high voltage pulses, 20 ns in duration (FWHM) with a 3 ns rise time, are delivered from a FPG20–03PN pulser (FID Technology) via the coaxial cable. A calibrated, custom-made back current shunt (BCS) [18] installed at midpoint along the length of this 30 m cable is used to measure the applied voltage on the high voltage electrode. Additional measurements are made to subtract the current associated with the charging of the capacitance of the electrode system. The chamber is filled with 5 bar of molecular nitrogen (N_2) for the E-FISH experiments.

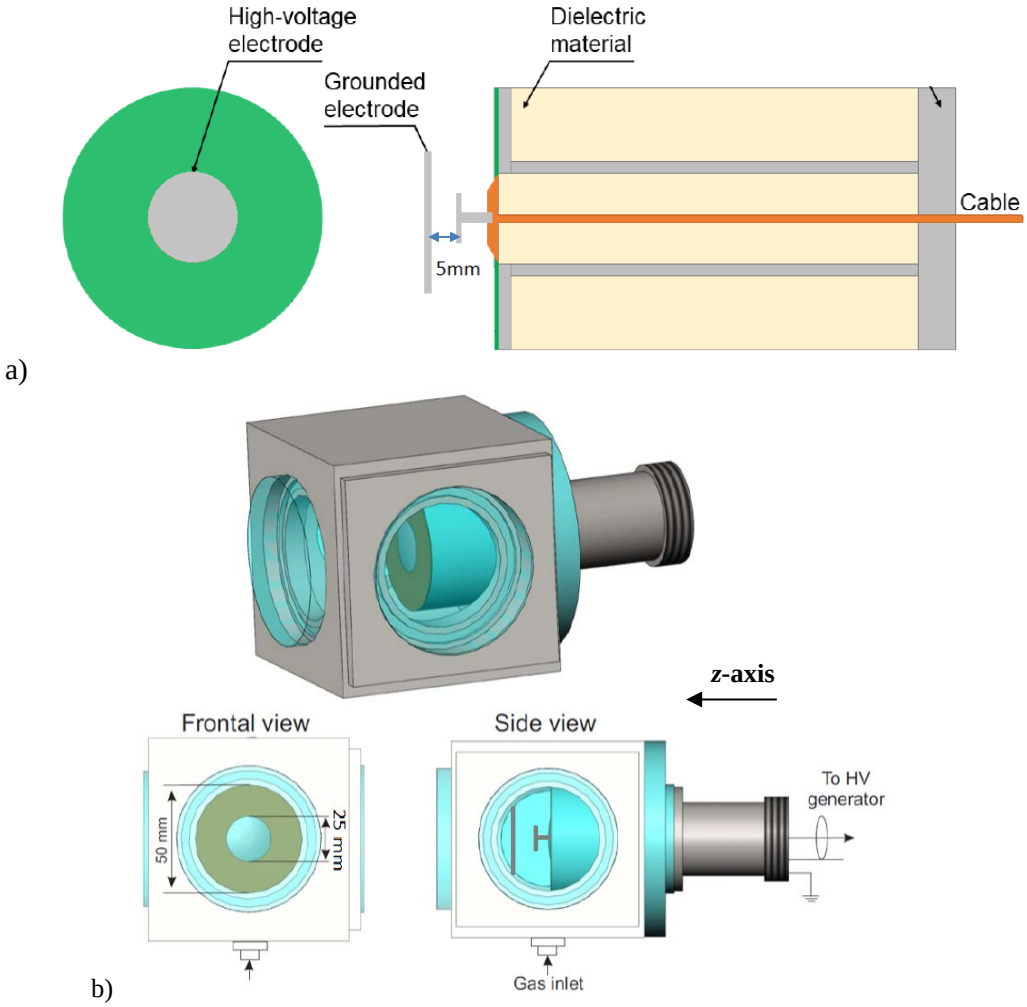

Figure 6. Schematic of the a) system of electrodes and b) high pressure, constant volume chamber.

3. Results of E-FISH experiments

The intensity of the vertically polarized 532 nm, E-FISH signal, $I_z^{(2\omega)}$, is given by,

$$I_z^{(2\omega)} = C \cdot \left[\chi^{(3)}(2\omega, 0, \omega, \omega) \cdot N \cdot E_z^{ext} \cdot I_z^{(\omega)} \cdot L\right]^2 \left[sinc\left(\frac{\Delta k \cdot L}{2}\right)\right]^2 \qquad (3)$$

In eqn. (2), E^{ext} represents the electric field to be measured, $I_z^{(\omega)}$ is the intensity of the vertically-polarized 1064 nm probe laser, $\chi^{(3)}$ is the third-order nonlinear susceptibility, N is the gas number density, L is the confocal beam parameter and Δk is the difference between the fundamental and second harmonic wave vectors. Here the z-axis is defined as the vertical axis, with z=0 corresponding to the location of the high-voltage electrode. Eqn. (2) is valid only for centrosymmetric media (i.e. no signal in the absence of an externally applied field) and is typically applied when the confocal beam parameter is smaller than the coherence length, L_c, where $L_c = \frac{\pi}{\Delta k}$. The coherence length at ambient pressure and temperature is about 6 cm, and to a good approximation, scales linearly with pressure. Thus, even at our working pressure of 5 bar, the estimated coherence length of about 1.1 cm is still larger than the confocal beam parameter of 2.4 mm.

Figure 7 plots the square root of the time-integrated E-FISH signals obtained from the electrostatic field together with the field values predicted by the BCS. These E-FISH signals are normalized by the time-integrated photodiode signals which provide a measure of the laser intensity. The applied voltage measured by the BCS is divided by the interelectrode gap distance of 5 mm to compute the electric field strength. For these experiments, the laser beam is focused at the center of the interelectrode gap. The E-FISH data (rescaled to fit the BCS field values) is observed to capture the shape of the applied high voltage pulse reasonably well, with slight discrepancies occurring during both the rise and fall of the pulse. This is to be expected given that the laser pulse width of ~3 ns (viz. measurement time resolution) is comparable to the rise time of the high voltage pulse. When conducting these experiments, no apparent contribution of the surface charges on the opposing quartz windows to the E-FISH signal is detected.

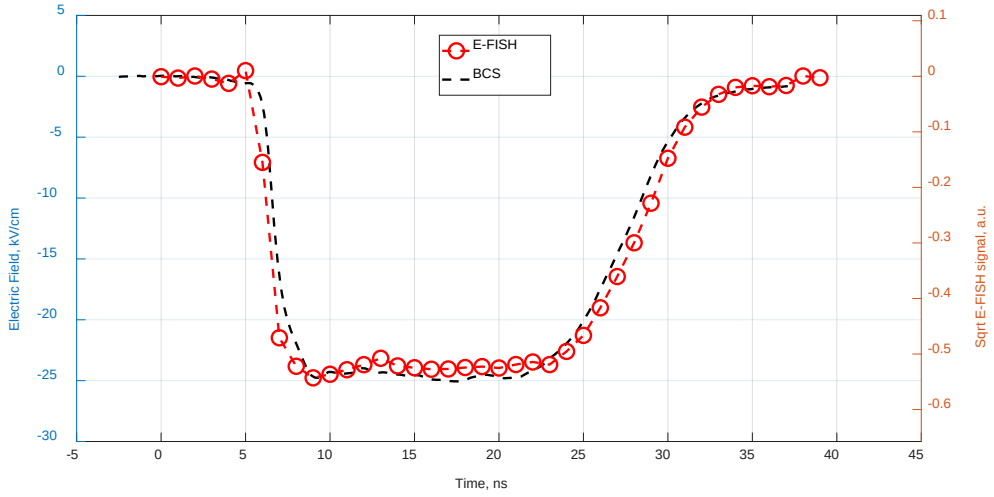

Figure 7. Plot of the square root of the E-FISH signal (normalized by the laser intensity) together with the electric field strength measured using a BCS. Each E-FISH data point corresponds to an average of 300 laser shots.

4. Conclusion

A Pockels-cell-based pulse slicing scheme has been successfully developed in this work for the purpose of performing electric field measurements using the E-FISH diagnostic. This slicing scheme is easily integrated with existing nanosecond laser systems and provides a robust and affordable method of carving out shorter optical pulses from a longer pulse. We integrate such a slicer with a conventional Nd:YAG nanosecond laser system, and utilize the resulting ~3 ns (FWHM), 2 mJ output to perform E-FISH tests in an above-atmospheric pressure, known electrostatic field. Further optimization of this slicer should readily result in higher output energies and shorter pulses on the order of 100 ps or less, and could serve as an effective tool for extending the benefits of ultrashort pulse operation to a wider audience.

Acknowledgments

The work was partially supported by French National Research Agency, ANR-16-CE30-0004 (ASPEN Project), LabEx Plas@Par and the French–Russian international laboratory LIA KaPPA 'Kinetics and Physics of Pulsed Plasmas and their Afterglow'. The authors would like to thank Dr. Jean-Paul Booth and Dr. Cyril Drag for the use of equipment essential for conducting these experiments, and Mhedine Ali Cherif for helpful contributions during the preparation of this manuscript. Internship support from the Vice Presidency for Marketing & International Relations (DMRI) for Maya Naphade and support from the Ecole Polytechnique Gaspard Monge Visiting Professor (GMVP) Program for Prof. Igor Adamovich is also gratefully acknowledged. Sandia National Laboratories is a multimission laboratory managed and operated by National Technology and Engineering Solutions of Sandia, LLC., a wholly owned subsidiary of Honeywell International, Inc., for the USDOE's National Nuclear Security Administration under contract DE-NA0003525.

References

[1] Finn, R. S., & Ward, J. F. (1974). Measurements of hyperpolarizabilities for some halogenated methanes. The Journal of Chemical Physics, 60(2), 454-458.

[2] Nahata, A., & Heinz, T. F. (1998). Detection of freely propagating terahertz radiation by use of optical second-harmonic generation. Optics letters, 23(1), 67-69

[3] Bigio, I.J., Finn, R.S. & Ward, J.F. (1975). Electric-field induced harmonic generation as a probe of the focal region of a laser beam. Applied optics, 14(2), pp.336-342.

[4] Dogariu, A., Goldberg, B. M., O'Byrne, S., & Miles, R. B. (2017). Species-independent femtosecond localized electric field measurement. Physical Review Applied, 7(2), 024024.

[5] Goldberg, B. M., Chng, T. L., Dogariu, A., & Miles, R. B. (2018). Electric field measurements in a near atmospheric pressure nanosecond pulse discharge with picosecond electric field induced second harmonic generation. Applied Physics Letters, 112(6), 064102.

[6] Chng, T. L., Orel, I. S., Starikovskaia, S. M., & Adamovich, I. V. (2019). Electric field induced second harmonic (E-FISH) generation for characterization of fast ionization wave discharges at moderate and low pressures. Plasma Sources Science and Technology, 28(4), 045004.

[7] Chng, T.L., Brisset, A., Jeanney, P., Starikovskaia, S.M., Adamovich, I.V. and Tardiveau, P. (2019). Electric field evolution in a diffuse ionization wave nanosecond pulse discharge in atmospheric pressure air. Plasma Sources Science and Technology.

[8] Simeni, M. S., Tang, Y., Frederickson, K., & Adamovich, I. V. (2018). Electric field distribution in a surface plasma flow actuator powered by ns discharge pulse trains. Plasma Sources Science and Technology, 27(10), 104001

[9] Goldberg, B. M., Reuter, S., Dogariu, A., & Miles, R. B. (2019). 1D time evolving electric field profile measurements with sub-ns resolution using the E-FISH method. Optics Letters, 44(15), 3853-3856.

[10] Becker, K.H., Kogelschatz, U., Schoenbach, K.H. and Barker, R.J. (2004). Non-equilibrium air plasmas at atmospheric pressure. CRC press.

[11] Starikovskiy, A. and Aleksandrov, N. (2013). Plasma-assisted ignition and combustion. Progress in Energy and Combustion Science, 39(1), pp.61-110.

[12] Favia, P. and d'Agostino, R. (1998). Plasma treatments and plasma deposition of polymers for biomedical applications. Surface and coatings Technology, 98(1-3), pp.1102-1106.

[13] Park, D.P., Davis, K., Gilani, S., Alonzo, C.A., Dobrynin, D., Friedman, G., Fridman, A., Rabinovich, A. and Fridman, G. (2013). Reactive nitrogen species produced in water by non-equilibrium plasma increase plant growth rate and nutritional yield. Current Applied Physics, 13, pp.S19-S29.

[14] Lagarkov, A.N. and Rutkevich, I.M. (2012). Ionization waves in electrical breakdown of gases. Springer Science & Business Media.

[15] Aleksandrov, N.L., Konchakov, A.M. and Son, E.E. (1978). Electron distribution function and kinetic coefficients of a nitrogen plasma. I-Unexcited molecules. *Soviet Journal of Plasma Physics*, *4*, pp.169-176.

[16] Pacala, T. J., Laudenslager, J. B., & Christensen, C. P. (1980). High-energy subnanosecond pulse amplification in XeCl. Applied Physics Letters, 37(4), 366-368.

[17] Ding, C., Khomenko, A.Y., Shcherbanev, S.A. and Starikovskaia, S.M. (2019). Filamentary nanosecond surface dielectric barrier discharge. Experimental comparison of the streamer-to-filament transition for positive and negative polarities. Plasma Sources Science and Technology, 28(8), p.085005.

[18] Anikin, N. B., Starikovskaia, S. M., & Starikovskii, A. Y. (2004). Study of the oxidation of alkanes in their mixtures with oxygen and air under the action of a pulsed volume nanosecond discharge. Plasma physics reports, 30(12), 1028-1042.